Molecular Imaging
Volume 16 : 1-9
© The Author(s) 2017
Reprints and permission:
sagepub.com/journalsPermissions.nav
DOI: 10.1177/1536012116689001
journals.sagepub.com/home/mix
SAGE

Image-Based Analysis of Tumor Localization After Intra-Arterial Delivery of Technetium-99m-Labeled SPIO Using SPECT/CT and MRI

In Joon Lee, MD, PhD[1], Ji Yong Park, MS[2,3], Young-il Kim, MD, PhD[2,4], Yun-Sang Lee, PhD[2,4], Jae Min Jeong, PhD[2], Jaeil Kim, BS[2], Euishin Edmund Kim, MD, PhD[4,5], Keon Wook Kang, MD, PhD[2], Dong Soo Lee, MD, PhD[2,4], Seonji Jeong, MD[6], Eun Jeong Kim, BS[6], Young Il Kim, MD, PhD[6,7], and Jin Wook Chung, MD, PhD[6]

Abstract

The aim of this study is to evaluate the localization of ^{99m}Tc-labeled dextran-coated superparamagnetic iron oxide (SPIO) nanoparticles to the liver tumor using image-based analysis. We delivered ^{99m}Tc-SPIO intravenously or intra-arterially (IA) with/without Lipiodol to compare the tumor localization by gamma scintigraphy, single-photon emission computed tomography (SPECT), and magnetic resonance imaging (MRI) in a rabbit liver tumor. The gamma and SPECT image-based analysis shows that the uptake ratio of the tumor to the normal liver parenchyma is highest after delivery of ^{99m}Tc-SPIO with Lipiodol IA and that well correlates with the trend of the signal decrease in the liver MRIs. Intra-arterial delivery of SPIO with Lipiodol might be a good drug delivery system targeting the hepatic tumors, as confirmed by image-based analysis.

Keywords

Intra-arterial (IA) delivery, technetium-99m, single-photon emission computed tomography (SPECT), superparamagnetic iron oxide (SPIO), magnetic resonance imaging (MRI)

Introduction

Hepatocellular carcinoma (HCC) is one of the most common cancers in the world.[1] The majority of patients diagnosed in intermediate or advanced stages are not amendable to curative resection.[2] Currently, transarterial chemoembolization (TACE) is the primary therapeutic option for the intermediate stage, which includes asymptomatic multifocal or large HCC according to the Barcelona Clinic Liver Cancer Classification.[3,4] Conventional TACE traditionally means that iodized oil is mixed with an anticancer drug and infused through the feeding artery of the HCC.[5,6] Ideally, the iodized oil acts like a drug-releasing carrier; therefore, it should be retained in the tumor tissue for a certain time to gradually release the anticancer drug within the tumor. Still, a significant amount of the infused anticancer drug passes into systemic circulation, which may cause systemic side effects.[7,8]

Superparamagnetic iron oxide (SPIO) is one class of magnetic nanoparticles that can play a role in drug-releasing nanocarriers, as well as serve as magnetic resonance imaging (MRI)

[1] Department of Radiology, National Cancer Center, Goyang-si, Gyeonggi-do, Republic of Korea
[2] Department of Nuclear Medicine, Seoul National University College of Medicine, Seoul, Republic of Korea
[3] Department of Transdisciplinary Studies, Program in Biomedical Radiation Science, Graduate School of Convergence Science and Technology, Seoul National University, Seoul, Republic of Korea
[4] Department of Molecular Medicine and Biopharmaceutical Sciences, Graduate School of Convergence Science and Technology, and College of Medicine or College of Pharmacy, Seoul National University, Seoul, Republic of Korea
[5] Department of Radiological Sciences, University of California, Irvine, USA
[6] Department of Radiology, Seoul National University Hospital, Seoul, Republic of Korea
[7] Department of Radiology, Sheikh Khalifa Specialty Hospital, Ras Al Khaimah, United Arab Emirate

Submitted: 27/04/2016. Revised: 12/12/2016. Accepted: 16/12/2016.

Corresponding Authors:
Yun-Sang Lee, 108 Medical Science Building, Seoul National University College of Medicine, 103 Daehak-ro, Jongno-gu, Seoul 03080, Republic of Korea.
Email: wonza43@snu.ac.kr
Jin Wook Chung, MD, Department of Radiology, Seoul National University Hospital, 101 Daehak-ro, Jongno-gu, Seoul 03080, Republic of Korea.
Email: chungjw@snu.ac.kr

contrast agents for clinical diagnosis.[9-13] Ferumoxide has been approved for use as a negative contrast agent in liver MRI because it creates a strong signal decrease in the normal liver parenchyma on the T2-weighted MRI.[14-16]

A recent experimental study reported that it was also able to act as a drug-releasing nanocarrier and could be applied as an intra-arterial (IA) drug delivery system in the TACE of the HCC.[17] A mixture of sticky oil, such as Lipiodol, and an anticancer drug-loaded ferumoxide could have pharmacokinetic advantages as well as being useful for the monitoring of the intratumoral accumulation of the infused mixture both by computed tomography (CT) and MRI.[17] However, that study had the lack of quantification data of the ferumoxide after IA delivery to liver tumor, even though this drug delivery system was a newly established one. Without knowing its whole-body distribution and pharmacokinetics, it is impossible to know how and where ferumoxide is distributed in the body after IA delivery.

A traditional biodistribution study of newly developed particles conventionally is carried out by sequentially killing the experimental animals at multiple time points after particle injection and measuring the amount of injected particles in each major organ. Several decades ago, ferumoxide was also evaluated using this method in clinical trials.[18] If particles can be labeled by a radioisotope, the image-based analysis of the localization of those particles could be demonstrated on nuclear medicine imaging modalities, such as gamma scintigraphy, single-photon emission computed tomography (SPECT), or positron emission tomography.

Research on radioisotope-labeled nanoparticles includes the monitoring of the in vivo behavior of nanoparticles to evaluate the feasibility of an in vivo application of those nanoparticles.[19-23] Through nuclear medicine imaging, the accumulation of nanoparticles in tumors and major organs at every time point could be obtained noninvasively and quantitatively. Technetium-99m is one of the commonly used radioisotopes in nuclear medicine with a 6-hour half-life, 140 keV gamma energy, and a generator-eluted radioisotope, which feature the most convenient method for clinical routines.[24] Referring to previous research on ^{99m}Tc-labeled dextran derivatives, we modified and used this method for radiolabeling of SPIO.[25]

In this study, we synthesized ^{99m}Tc-labeled SPIO and delivered those nanoparticles to liver tumor–bearing rabbits intravenously (IV) or IA with/without Lipiodol and compared the tumor localization of those particles using image-based analysis.

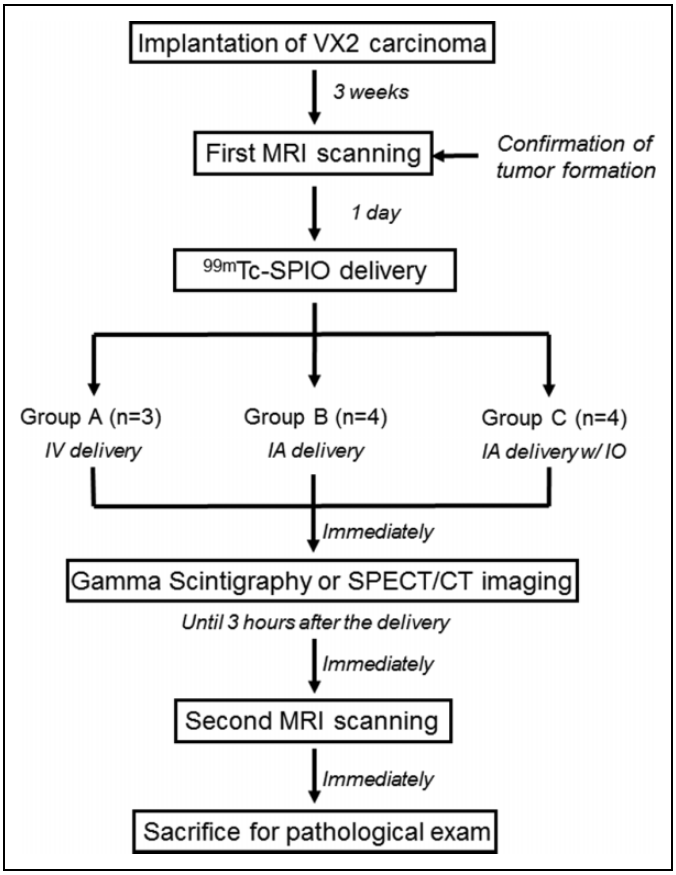

Figure 1. Overview of the experimental design.

Materials and Methods

General

Commercially available dextran-coated SPIO nanoparticles (MR contrast agent, Feridex IV, core size: 5-10 nm, overall size: 100-250 nm; Advanced Magnetics, Cambridge, Massachusetts) were used for this experiment.[26] Lipiodol was purchased from Andre Guerbet (Aulnay-sous-Bois, France) and a desalting column was from GE Healthcare Bio-Sciences Corp (PD-10, Sephadex G-25 Medium, New Jersey). Tiletamine–zolazepam (Zoletil 50; Virbac, Carros, France) and xylazine hydrochloride (Rompun; Bayer, Seoul, South Korea) were used for anesthetic agents. ^{99}Mo-^{99m}Tc generator (Samyong Unitech Co, Seoul, South Korea) was used for ^{99m}Tc elution. A microcatheter (Progreat; Terumo, Tokyo, Japan) was used for IA delivery procedures.

All other reagents were purchased from Sigma-Aldrich Korea (Gyeonggi Province, South Korea) and were used without further purification. Particle size distribution was measured by nanotracking analysis (NTA) method using a NANOSIGHT instrument (Malvern, United Kingdom). The radiolabeling yield or the purity of the ^{99m}Tc-SPIO was checked by thin-layer chromatography (TLC) using ITLC-SG (Agilent Technologies, Lake Forest City, California) as a stationary phase and acetone or 0.1 M citrate solution as a mobile phase. Radio chromatograms were obtained using an AR2000 TLC scanner (Bioscan, Washington, DC). Magnetic resonance images were obtained using a 3.0-T Tim Trio clinical MRI scanner (Siemens Healthcare, Erlangen, Germany), and images were analyzed on a Picture Archiving and Communications System (PACS) workstation (m-view; Marotech, Seoul, Korea); SPECT/CT images and scintigraphy images were obtained using a GE Discovery model NM/CT 670 instrument (GE Healthcare, Milwaukee, Wisconsin). Visipaque 270 (GE Healthcare Ireland, Cork, Ireland) was used as CT contrast media. SPSS version 16.0 (SPSS, Inc, an IBM Company, Chicago, Illinois) was used for statistical analysis.

The study was approved both by the Institutional Animal Care and Use Committee (No. 13-0059) and the Institutional Biosafety Committee (No. 1303-006-004) at Seoul National University Hospital.

Study Design and Animal Model

The scheme of the experimental design is shown in Figure 1. Adult New Zealand white rabbit was selected as an experimental model of liver cancer. VX2 carcinoma is an anaplastic squamous cell carcinoma derived from a virus-induced papilloma in rabbits, and we selected the rabbit VX2 liver tumor model as an experimental model in this study, which is widely known for well-established animal model for the study of TACE because its blood supply is similar to that of HCC. The VX2 carcinoma strain was maintained in the right hind limb of a carrier rabbit by deep intramuscular injection throughout the study.[27,28]

A total of 12 rabbits weighing 3.0 to 3.5 kg were raised in rooms with a 12-hour light/dark cycle and a constant temperature (23°C ± 2°C). One rabbit was missed by overdose of anesthetic agent. Anesthesia was induced with an intramuscular injection of 5 mg/kg body weight tiletamine–zolazepam and 2 mg/kg body weight 2% xylazine hydrochloride for all procedures. The left lobe of the liver was exposed through a midline incision in the abdominal wall, and a small piece of tumor (1 mm^3, VX2 carcinoma) was directly implanted at the subcapsular area.[17,29] Tumor formation was confirmed by MRI obtained at 3 weeks after tumor implantation.

^{99m}Tc-SPIO was administered to the rabbit tumor model using 3 different methods: group A (n = 3) underwent IV delivery of a mixture of 0.2 mL of ^{99m}Tc-SPIO and 0.25 mL of normal saline via the left auricular vein, group B (n = 4) underwent delivery of a mixture of 0.2 mL of ^{99m}Tc-SPIO and 0.25 mL of contrast media (Visipaque) through the hepatic artery, and group C (n = 4) underwent delivery of a mixture of 0.2 mL of ^{99m}Tc-SPIO and 0.25 mL of Lipiodol through the hepatic artery. The radioactivity, 2.55 ± 0.04 MBq (70 ± 1.1 μCi), and the iron content were the same for all groups in the total injected volume. Scintigraphy was sequentially performed as 1-minute time frames for 20 minutes and then static images were obtained at 60 and 180 minutes and SPECT/CT imaging was performed at 90 minutes after the delivery of ^{99m}Tc-SPIO. Finally, after the second MR scanning, pathological specimens were acquired to confirm the presence of SPIO in the tumor.

Synthesis of ^{99m}Tc-SPIO

For the image-based biodistribution study, ^{99m}Tc-SPIO was prepared using the previously reported method, with a few modifications (Figure 2A).[25] Briefly, 1.5 mL of Feridex IV solution (30.45 mg of SPIO) was reacted with the mixture of $NaIO_4$ (3.9 mg, 0.018 mmol) and H_2SO_4 (2 μL), and the mixture was vortexed and kept at room temperature for 30 minutes. The resulting reaction mixture was purified on a desalting column, which was equilibrated with distilled water before use. Ten serial fractions (10 × 0.5 mL) were collected, and the 5 colored fractions were combined and used for the next reaction. The purified SPIO derivatives in distilled water (2.5 mL, 0.18 μmol) was mixed with 100-fold molar excess of cysteamine (2.1 mg, 0.018 mmol), and the mixture was stirred at room temperature for 60 minutes. Then, sodium borohydride ($NaBH_4$, 0.687 mg, 0.018 mmol) was added, and the resulting reaction mixture was stirred for 60 minutes in an ice-cold water bath. The final reaction mixture was neutralized with 1 M hydrochloric acid and purified once again using a desalting column (PD-10). The cysteamine-modified SPIO was kept at 4°C before ^{99m}Tc labeling. Particle size was checked by NTA before and after modifications. The amount of Fe (mg Fe/kg) of the cysteamine-modified SPIO, which was injected into each rabbit, was calculated from the standard curve of the particle number count of the serially diluted standard SPIO solution using NTA.

Technetium-99m labeling was performed by a reported method[30] with little modification as follows: $^{99m}TcO_4^-$ was eluted from a ^{99}Mo–^{99m}Tc generator with sterile saline. Aliquot solution of the cysteamine-modified SPIO (0.2 mL, 3.73 mg/mL) was mixed with $SnCl_2{\cdot}2H_2O$ (10 μL, 2.5 mg/mL) in 0.1 M HCl, then freshly eluted by adding 3.7 MBq (100 μCi) of $^{99m}TcO_4^-$ (15-20 μL) to the mixture, and was allowed to stand for 30 minutes at 37.5°C in a shaking incubator. The resultant was purified by the PD-10 column to remove other small molecules and free-^{99m}Tc.

The labeling efficiency of the ^{99m}Tc-labeled SPIO was checked by TLC using ITLC-SG as a stationary phase and acetone or 0.1 M citrate as a mobile phase. To distinguish ^{99m}Tc-SPIO from ^{99m}Tc-tin-colloid, we synthesized ^{99m}Tc-tin-colloid, which could be formed without a ^{99m}Tc chelator, and compared the R_f values in the TLC with that of ^{99m}Tc-SPIO.

Magnetic Resonance Imaging Scanning and Analysis

All animals were scanned by MRI twice: 1 day before the delivery of ^{99m}Tc-SPIO (first MRI) and after the acquisition of the nuclear images (second MRI). A 3.0-T clinical MR scanner (with a knee coil to improve the resolution) was used. To reduce any artifact due to movement, an abdominal bandage was tightly applied to all animals. Axial T2-weighted turbo spin-echo (repetition time, milliseconds/echo time, milliseconds, 4100/150; echo train length, 14; 3-mm section thickness; Field of view [FOV], 130 × 130 mm; matrix, 512 × 358; and Number of excitations [NEX], 2.0) and T2*-weighted gradient-echo images were obtained (repetition time, milliseconds/echo time, milliseconds, 113/10; flip angle, 20°; section thickness, 3 mm; FOV, 136 × 136 mm; matrix, 320 × 320; and NEX, 10.0).

Magnetic resonance imaging images were analyzed on PACS workstation by a radiologist. The maximal longitudinal diameters of the tumors were determined from the T2-weighted images. The relative tumor–back muscle signal intensity ratios were calculated by a reported method[17] from the signal intensity of the tumor and back muscles in the same plane of the first and second MRI T2*-weighted images.

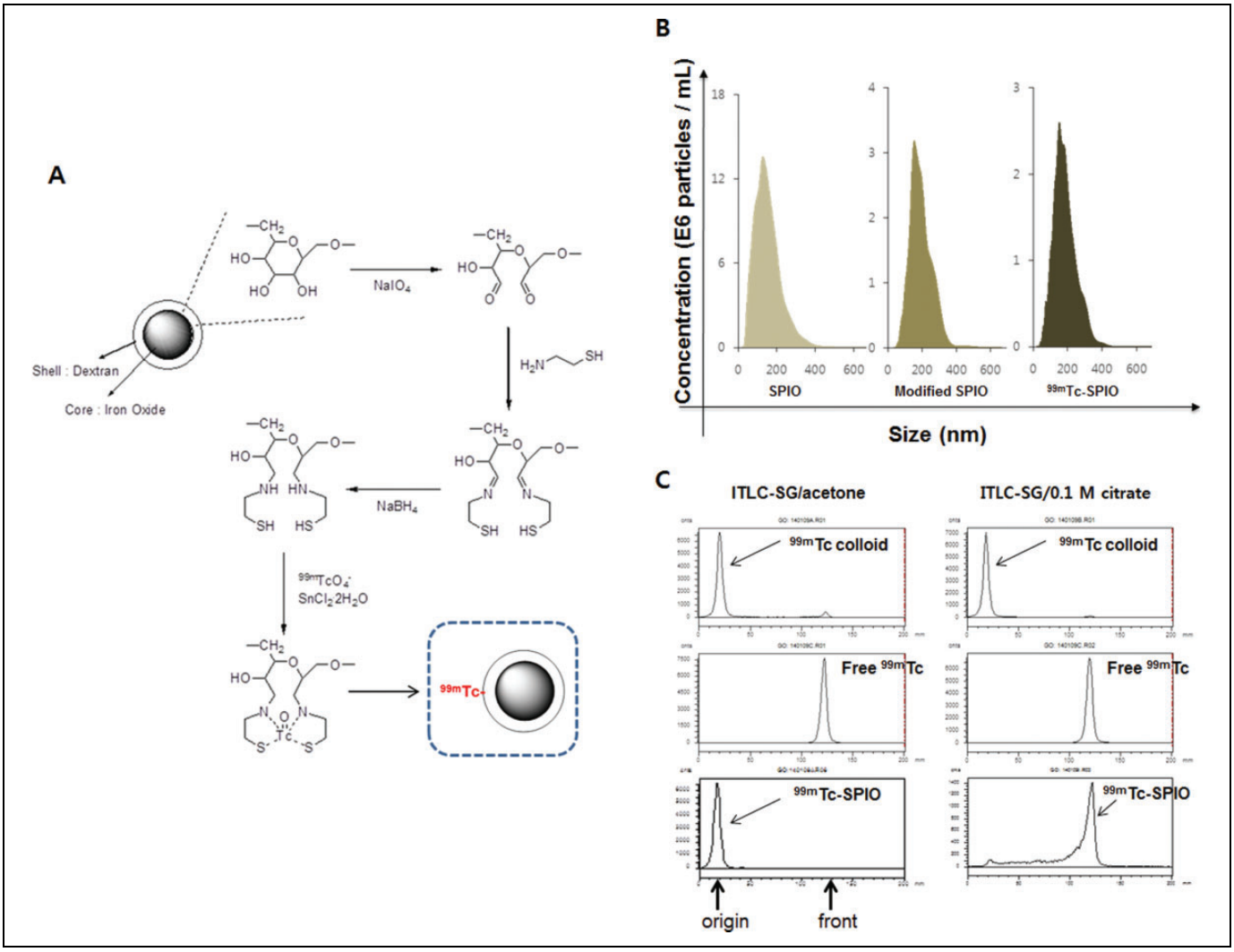

Figure 2. The surface modification and ^{99m}Tc labeling of SPIO: The schematic procedure for the surface modification of SPIO and ^{99m}Tc labeling (A); the size distribution of the SPIO, the modified SPIO, and the ^{99m}Tc-SPIO (B); radiochromatograms of ^{99m}Tc-SPIO (C). SPIO indicates superparamagnetic iron oxide.

Intra-Arterial Delivery Procedure

All IA delivery procedures were performed by an interventional radiologist. An 18-gauge IV catheter was inserted into the right auricular artery, and a microcatheter was advanced through this route to the descending aorta and celiac axis.[31,32] Hepatic arteriography was performed to identify the tumor location and its feeder from the left hepatic artery. After the microcatheter was successfully navigated to the feeder, the materials prepared for the particular study group were carefully infused while avoiding retrograde reflux into the right hepatic artery.

Gamma Scintigraphy and SPECT/CT Image Acquisition and Analysis

After the delivery of ^{99m}Tc-SPIO (200 μL, 0.25 mg Fe/kg, 2.55 ± 0.04 MBq), the animals were placed into a SPECT/CT scanner and immediately underwent a dynamic scan with a gamma scintigraphy image using 1-minute time frames for 20 minutes. Static scintigraphy images were obtained at 60 and 180 minutes after the delivery. The gamma scintigraphy images were acquired with a low-energy, high-resolution collimator (10% window centered at 140 keV, ×1.28 zoom, and a 256 × 256 matrix) using the step-and-shoot scan mode. Single-photon emission computed tomography/CT scanning was performed 90 minutes after the delivery of ^{99m}Tc-SPIO for each group. Computed tomography and SPECT images were acquired for 10 and 20 minutes, respectively. Computed tomography scanning was performed using the following parameters: 16 × 0.625 mm detector configuration, a rotation time of 1 second, 0.562 pitch, 120 kVp, 30 mAs, 1.25-mm slice thickness with no gap, and 512 × 512 matrix size. Single-photon emission computed tomography images were taken using a low-energy, high-resolution collimator, 10% window centered at 140 keV, 2-mm slice thickness, ×1.0 zoom, and a

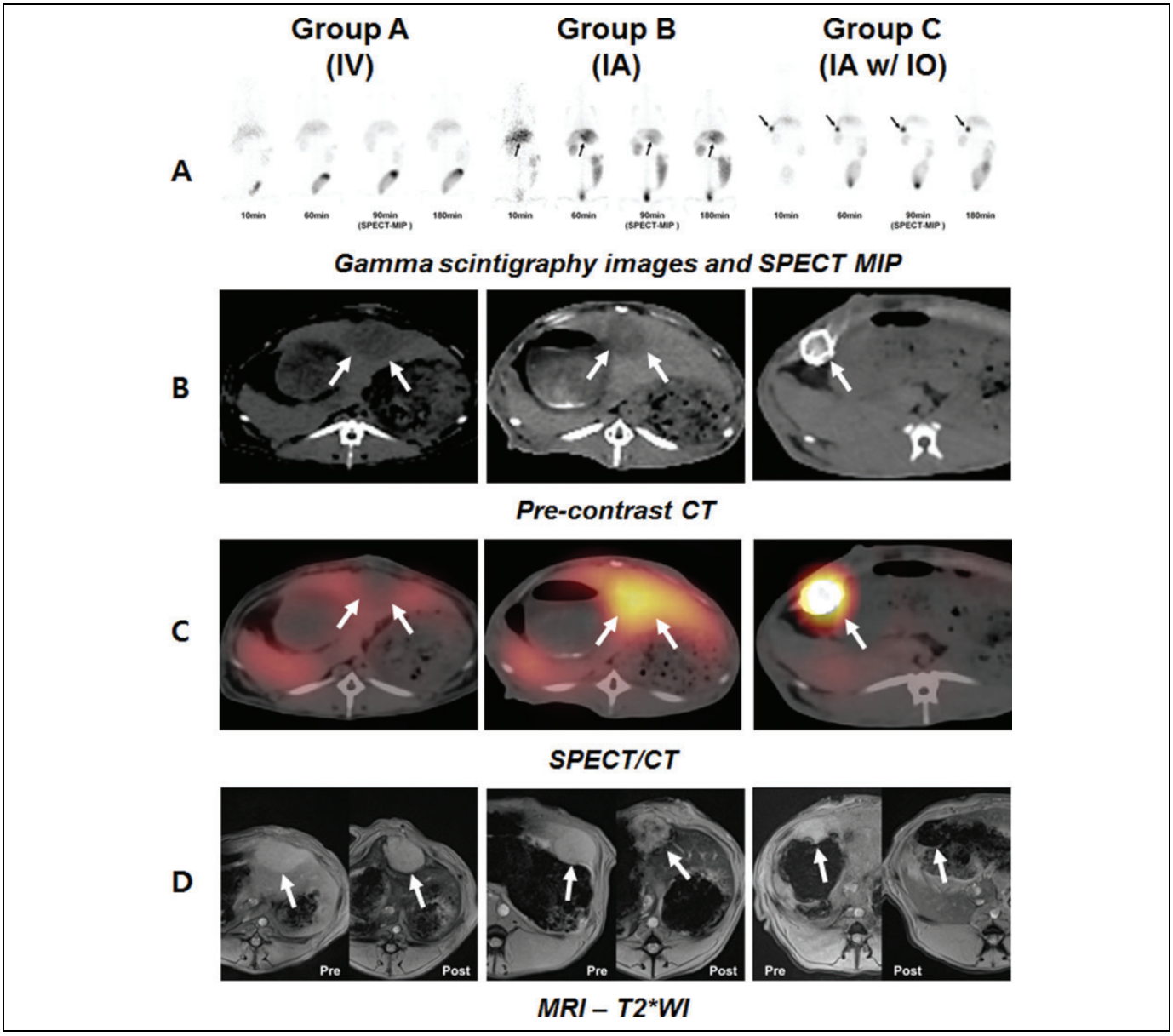

Figure 3. A, Tumor localization images of ^{99m}Tc-SPIO: Gamma scintigraphy and SPECT MIP (maximum intensity projection); (B) Pre-contrast CT; (C) SPECT/CT; (D) T2*-weighted images pre- or postdelivery of ^{99m}Tc-SPIO. CT indicates computed tomography; SPECT, single-photon emission computed tomography; SPIO, superparamagnetic iron oxide.

128 × 128 matrix with the step-and-shoot scan mode. Gamma scintigraphy and SPECT/CT images were reconstructed by the ordered subset expectation maximization (iteration = 2, subset = 10) with a Butterworth filter (frequency = 0.48, power = 10). The fusion of the SPECT and CT images was performed automatically by the software.

For the analyses of the SPECT/CT images, a nuclear medicine physician drew a volume of interest (VOI) for the CT-matched tumor lesion for maximum tumor count identification using the GE workstation. A VOI of normal liver parenchyma was also drawn and confirmed the mean count as background. For gamma scintigraphy image analysis, a nuclear medicine physician drew a region of interest (ROI) for SPECT/CT-matched tumor lesion area and checked the maximum tumor count. The ROI of normal liver parenchyma was drawn and verified the mean count as background.

The CT images were evaluated on the same workstation by a radiologist. The high attenuated lesions in the tumors suggested iodized oil accumulation. The CT attenuation values of the iodized oil accumulated in the tumor and normal liver parenchyma were measured.

Pathological Analysis

Experimental animals were killed using IV injection of a lethal amount (7-10 mL) of xylazine hydrochloride under

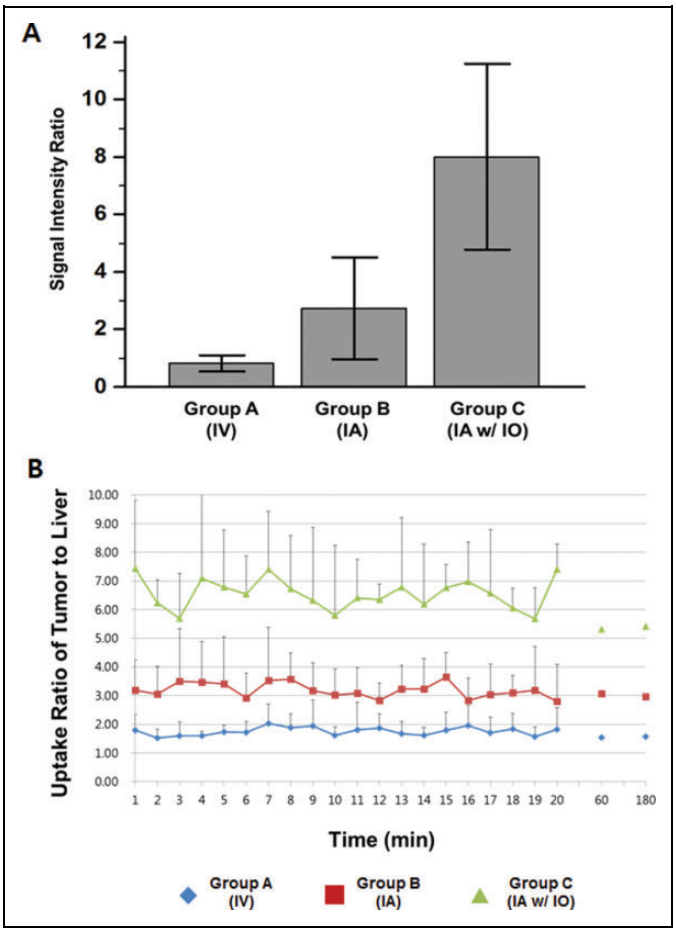

Figure 4. The image-based analysis of tumor localization of ^{99m}Tc-SPIO. A, The uptake ratio of the tumor to the normal liver parenchyma on the ^{99m}Tc-SPIO SPECT/CT at 90 minutes after delivery (positive results [$P < .05$] in the post hoc test: A vs B [$P = .032$], A vs C [$P = .032$], B vs C [$P = .043$]. B, The uptake ratio of tumors to the normal liver parenchyma on the ^{99m}Tc-SPIO scintigraphy images after 180 minutes. CT indicates computed tomography; SPECT, single-photon emission computed tomography; SPIO, superparamagnetic iron oxide.

deep anesthesia. Livers were carefully removed, the tumors and the right hemiliver parenchyma were placed in a bottle containing 5% formalin and subsequently treated with hematoxylin and eosin staining for basic histopathological examinations, and then Prussian blue staining was applied to confirm SPIO deposition.

Statistical Analysis

Data processing and analysis were performed using SPSS version 16.0. The Kruskal-Wallis test was conducted to compare the tumor size and the uptake ratio of the tumor to normal liver parenchyma on the gamma scintigraphy images and the signal intensity ratio of the tumor to the back muscles on the MRI images. The Mann-Whitney *U* test was used for 1-to-1 group comparisons as a post hoc test of the nonparametric test. Two-tailed *P* values <.05 were considered as statistically significant.

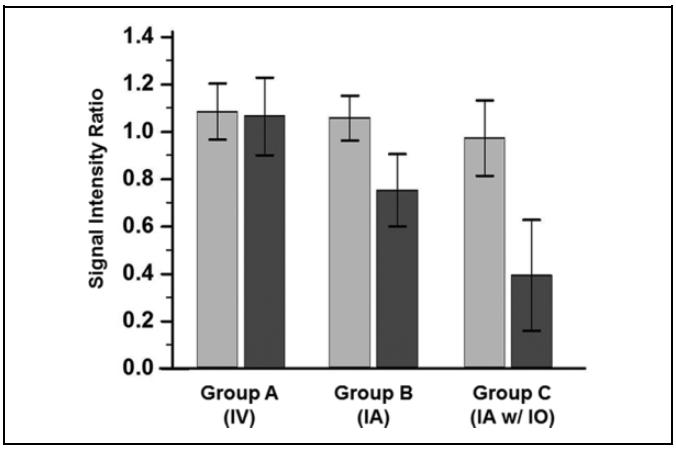

Figure 5. Signal decreases of the tumor on second MRIs at 3 hours after delivery (first MRIs: gray bar; second MRIs: dark gray bar; positive results in the post hoc test for second MRIs: A vs C ($P < .001$), B vs C ($P < .001$). MRI indicates magnetic resonance imaging.

Results

Characterization of ^{99m}Tc-SPIO

The size of the SPIO, the modified SPIO, and the ^{99m}Tc-SPIO were measured by NTA to be 158 ± 60 nm, 168 ± 67 nm, and 155 ± 65 nm, respectively (Figure 2B). The labeling efficiency as well as radiochemical purity of ^{99m}Tc-SPIO was measured by radio-TLC to be >95% (Figure 2C). The final Fe amount and radioactivity of ^{99m}Tc-SPIO, which was injected into each rabbit, were calculated to be 0.25 mg Fe/kg and 2.55 ± 0.04 MBq. The stability of ^{99m}Tc-SPIO in human serum at 37°C was checked by radio-TLC and over 90% for 2 hours (data were not shown).

^{99m}Tc-SPIO Scintigraphy and SPECT/CT Image-Based Analysis

Figure 3 presents representative scintigraphy, SPECT/CT, and MRIs for each group. Group C shows the highest tumor uptake of ^{99m}Tc-SPIO among the studied groups in scintigraphy images and SPECT/CT images, and persistent retention can be observed from the initial image to the image taken at 180 minutes (Figure 3A and B). The tumor-to-normal liver parenchyma uptake ratios on SPECT/CT images were significantly different between all 3 groups and ranged in the order of C > B > A (Kruskal-Wallis test, $P < .05$; Figure 4A), which correlated well with the signal decrease trend shown on the liver MRIs (Figure 5). On the CT images, only group C showed iodized oil uptake in the tumor (Figure 3B).

Signal Intensity of Tumors in MRI

Measured diameters of the tumors were 1.8 ± 0.61 cm (mean ± standard deviation [SD]) for group A, 1.6 ± 0.17 cm for group B, and 1.6 ± 0.32 cm for group C. There was no significant difference in tumor size among the groups ($P = .919$).

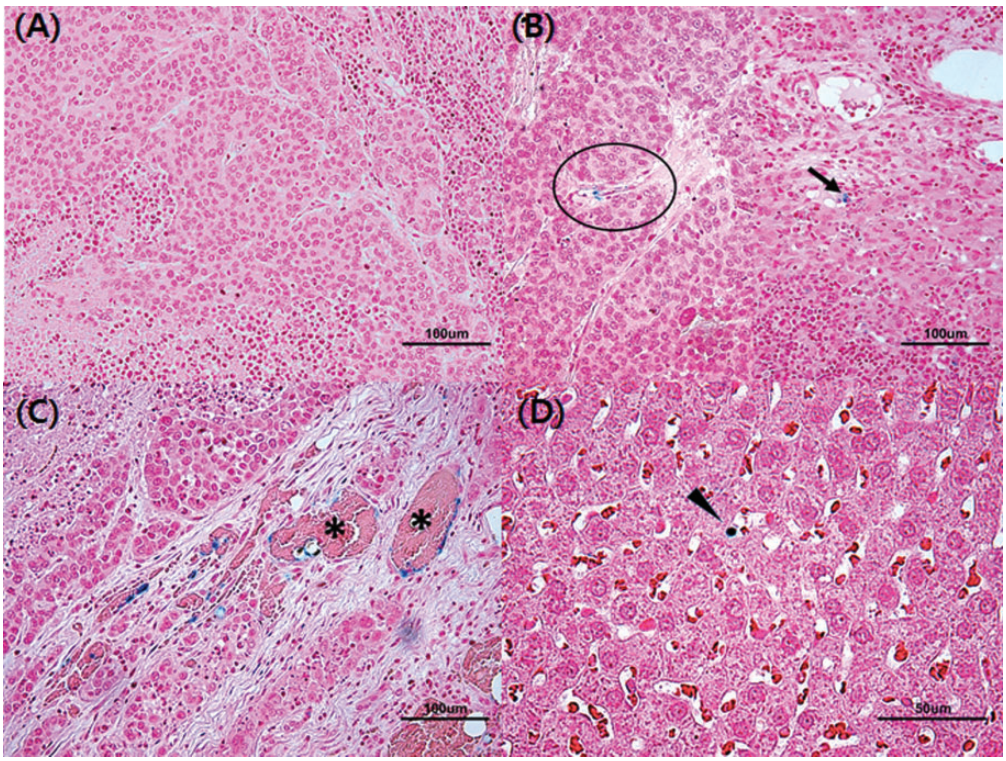

Figure 6. Photograph of Prussian blue staining: ×200 image in group A. A, There is no Prussian blue–positive vesicles in the tumor, ×200 images in group B. B, Prussian blue–positive vesicles (blue color) are deposited in the septum (circle) and the tumor cell (arrow), ×200 image in group C. C, Prussian blue–positive vesicles (blue color) is frequently demonstrated around occluded tumor vessels filled with blood clots (stars), ×400 image in normal liver parenchyma. D, A small cell (arrow head) suggested Kupffer cell contains Prussian blue–positive vesicles (blue color).

In T2*-weighted gradient-echo images, group C showed the highest signal decrease after ^{99m}Tc-SPIO delivery to the tumor tissue; in contrast, group A showed no significant MR signal change after ^{99m}Tc-SPIO delivery (Wilcoxon rank sum test, $P = 1.0$; Figure 3D).

In comparison between groups A, B, and C, there were no differences in the first set of MRIs, but the signal/intensity ratio was significantly different between groups for second MRIs (Kruskal-Wallis test, $P < .05$ for the second MRIs, $P > .1$ for the first MRIs; Figure 5). According to the relative tumor–back muscle signal intensity ratio, group C exhibited the most signal decrease in the tumor on second MRIs and there were significant differences in group C versus groups B and A ($P < .001$; Figure 5).

Pathological Examination

In groups B and C, Prussian blue–positive vesicles (indicating the presence of Fe^{2+} ions) were identified around tumor vessels, and in a few tumor cells, a septum within the tumor and a capsule of the tumor (Figure 6). Group C had Prussian blue–positive lesions more frequently than group B, mainly around the tumor vessels. However, no Prussian blue–positive lesions were observed in the tumors of group A. In the right hemiliver parenchyma of all of the groups, a few cells contained Prussian blue–positive vesicles representing Kupffer cells were identified.

Discussion

Radioisotope-labeled nanoparticles may be used for multimodal imaging to overcome the limitations of each imaging modality.[33] We used ^{99m}Tc-SPIO as a multimodal imaging agent to evaluate the biodistribution of dextran-coated SPIO nanoparticles allowing to acquire sensitive and quantitative SPECT data and high spatial resolution MRI images.

Dextran-coated SPIO nanoparticles were successfully modified using a ring-opening reaction of a glucose moiety of dextran for the conjugation of cysteamine, and a sodium borohydride reduced Schiff base to the secondary amine, and finally, we obtained the chelator-modified SPIO for ^{99m}Tc labeling. The size of the SPIO did not significantly change after surface modification and radiolabeling; therefore, we expected that the tumor localization pattern of the SPIO and ^{99m}Tc-SPIO would be the same. Technetium-99m labeling of the modified SPIO was performed using the conventional method ($SnCl_2$-reducing agent). Labeling efficiency and radiochemical purity were measured by radio-TLC to be over 95%. In the radio-TLC, ^{99m}Tc-SPIO moved with the solvent front (R_f value: 1.0), whereas the ^{99m}Tc-tin-colloid remained at the origin (R_f value: 0) in the 0.1 M citrate eluent (Figure 2C). The final product contained less than 2% of ^{99m}Tc-tin-colloid and was used without further purification.

As a result, sequential, noninvasive, and quantitative tumor localization assessment was achieved using the various

delivery methods. Our method can be applied in an image-based tumor localization analysis of newly developed SPIO agents.

The uptake ratio of tumor to normal liver calculated from the scintigraphy images was more than 1 in group A (Figure 4B), whereas from SPECT/CT, data were less than 1 (Figure 4A). We believe that the overlap of the normal liver parenchyma with the tumor hampers the exact evaluation of the ^{99m}Tc-SPIO distribution by gamma scintigraphy. Future studies of newly developed SPIO should include SPECT/CT imaging for accurate analyses.

The average size of the ^{99m}Tc-SPIO was 155 nm and much smaller than liver capillary, thus ^{99m}Tc-SPIO could easily leak from the tumor after IA delivery. In this study, group C (IA delivery with Lipiodol) had the highest tumor retention among 3 groups according to ^{99m}Tc-SPIO scintigraphy, SPECT/CT, and MRIs. And also more iron depositions or Fe ions were found, mainly around the perivascular structures on the pathology slides. The iodized oil blocks the blood flow of the tumor-feeding artery in chemoembolization,[34] which may result in better SPIO retention in the tumor, especially around the tumor vessels. Moreover, for hypervascular tumors, the blockage of tumor-feeding arteries creates ischemia of the tumor and results in necrosis; therefore, a combination of SPIO and Lipiodol in the IA delivery system can maximize drug delivery to the tumor and consequently the therapeutic response.

Evaluating the accumulation of the chemoembolic materials in the tumor is important, because it allows prediction of the therapeutic response. Computed tomography scans are usually used for evaluation after chemoembolization with Lipiodol, because the iodized oil has a strong CT contrast. Recently, MRI has been widely used as the imaging modality of choice in patients with liver cancers, because it can detect HCC better than CT.[35] However, it is hard to detect Lipiodol deposition on MRIs because of the vague signal intensity changes in the tumor.[36] In this study, we could monitor the delivery of chemoembolic materials (^{99m}Tc-SPIO with Lipiodol, group C) by fluoroscopy guidance and by nuclear medicine imaging modalities, CT, MRI, or multimodal detection.

In this study, we observed that normal liver had slight signal decreases in liver MRIs and diffuse uptake on scintigraphy and SPECT images at 3 hours after IA delivery of ^{99m}Tc-SPIO with or without Lipiodol. That may result from the deposition of SPIO passing into the systemic circulation. Feridex could easily be taken up in healthy liver and spleen tissues.[18] Therefore, off-target delivery also should be considered in future studies, as this effect could be problematic because of potential hepatotoxicity. The kidneys and bladders also show diffuse uptake on ^{99m}Tc-SPIO scintigraphy and SPECT images, but there is no signal decrease for MRIs. Referring to the literature, Feridex is seldom retained in these organs.[18] Therefore, this uptake might not be related to the deposition of SPIO. As the thyroid gland did not show high uptake, the diffuse uptake is also not related to free ^{99m}Tc. In our speculation, the kidney and bladder uptake might come from the detached ^{99m}Tc-chelator moiety, not from the free ^{99m}Tc, by the degradation of the ^{99m}Tc-chelator moiety on the surface of the SPIO, which would be excreted through urinary track.

In conclusion, we successfully demonstrated the image-based tumor localization of ^{99m}Tc-SPIO in VX2 tumor model, and the IA delivery of SPIO/Lipiodol mixture was confirmed to be a potential drug delivery system targeting liver tumors.

Authors' Note

Informed consent was obtained from all individual participants included in the study. The first three authors contributed equally to this work.

Acknowledgments

The authors acknowledge Dr Lojos Balogh for help with the revision of this manuscript.

Declaration of Conflicting Interests

The author(s) declared no potential conflicts of interest with respect to the research, authorship, and/or publication of this article.

Funding

The author(s) disclosed receipt of the following financial support for the research, authorship, and/or publication of this article: This study was supported by a grant from the Korean Health Technology R&D Project through the Korea Health Industry Development Institute (KHIDI), funded by the Ministry of Health & Welfare, Republic of Korea (HI12C1148, HI14C1277 and HI15C3093), and the National Research Foundation of Korea (NRF-2015M2A2A7062450).

References

1. Jemal A, Bray F, Center MM, Ferlay J, Ward E, Forman D. Global cancer statistics. *CA Cancer J Clin*. 2011;61(2):69–90.
2. Kim YI, Park JW, Kwak HW, et al. Long-term outcomes of second treatment after initial transarterial chemoembolization in patients with hepatocellular carcinoma. *Liver Int*. 2014;34(8): 1278–1286.
3. Bruix J, Sherman M. Management of hepatocellular carcinoma. *Hepatology*. 2005;42(5):1208–1236.
4. Forner A, Llovet JM, Bruix J. Hepatocellular carcinoma. *Lancet*. 2012;379(9822):1245–1255.
5. Chung JW, Kim HC, Yoon JH, et al. Transcatheter arterial chemoembolization of hepatocellular carcinoma: prevalence and causative factors of extrahepatic collateral arteries in 479 patients. *Korean J Radiol*. 2006;7(4):257–266.
6. Lee IJ, Chung JW, Kim HC, et al. Extrahepatic collateral artery supply to the tumor thrombi of hepatocellular carcinoma invading inferior vena cava: the prevalence and determinant factors. *J Vasc Interv Radiol*. 2009;20(1):22–29.
7. Johnson PJ, Kalayci C, Dobbs N, et al. Pharmacokinetics and toxicity of intraarterial adriamycin for hepatocellular carcinoma: effect of coadministration of lipiodol. *J Hepatol*. 1991;13(1): 120–127.
8. Varela M, Real MI, Burrel M, et al. Chemoembolization of hepatocellular carcinoma with drug eluting beads: efficacy and doxorubicin pharmacokinetics. *J Hepatol*. 2007;46(3):474–481.

9. Cole AJ, Yang VC, David AE. Cancer theranostics: the rise of targeted magnetic nanoparticles. *Trends Biotechnol*. 2011;29(7): 323–332.
10. Ittrich H, Peldschus K, Raabe N, Kaul M, Adam G. Superparamagnetic iron oxide nanoparticles in biomedicine: applications and developments in diagnostics and therapy. *Rofo*. 2013; 185(12):1149–1166.
11. Sun C, Lee JS, Zhang M. Magnetic nanoparticles in MR imaging and drug delivery. *Adv Drug Deliv Rev*. 2008;60(11):1252–1265.
12. Veiseh O, Gunn JW, Zhang M. Design and fabrication of magnetic nanoparticles for targeted drug delivery and imaging. *Adv Drug Deliv Rev*. 2010;62(3):284–304.
13. Zhang XY, Robledo BN, Harris SS, Hu XP. A bacterial gene, mms6, as a new reporter gene for magnetic resonance imaging of mammalian cells. *Mol Imaging*. 2014;13.
14. Stark DD, Weissleder R, Elizondo G, et al. Superparamagnetic iron oxide: clinical application as a contrast agent for MR imaging of the liver. *Radiology*. 1988;168(2):297–301.
15. Oswald P, Clement O, Chambon C, Schouman-Claeys E, Frija G. Liver positive enhancement after injection of superparamagnetic nanoparticles: respective role of circulating and uptaken particles. *Magn Reson Imaging*. 1997;15(9):1025–1031.
16. Benderbous S, Corot C, Jacobs P, Bonnemain B. Superparamagnetic agents: physicochemical characteristics and preclinical imaging evaluation. *Acad Radiol*. 1996;3(suppl 2):S292–S294.
17. Lee IJ, Ahn CH, Cha EJ, Chung IJ, Chung JW, Kim YI. Improved drug targeting to liver tumors after intra-arterial delivery using superparamagnetic iron oxide and iodized oil: preclinical study in a rabbit model. *Invest Radiol*. 2013;48(12):826–833.
18. Weissleder R, Stark DD, Engelstad BL, et al. Superparamagnetic iron oxide: pharmacokinetics and toxicity. *AJR Am J Roentgenol*. 1989;152(1):167–173.
19. de Rosales RTM, Tavare R, Glaria A, Varma G, Protti A, Blower PJ. Tc-99m-bisphosphonate-iron oxide nanoparticle conjugates for dual-modality biomedical imaging. *Bioconjug Chem*. 2011; 22(3):455–465.
20. Lee HY, Li Z, Chen K, et al. PET/MRI dual-modality tumor imaging using arginine-glycine-aspartic (RGD)-conjugated radiolabeled iron oxide nanoparticles. *J Nucl Med*. 2008;49(8):1371–1379.
21. Lee YK, Jeong JM, Hoigebazar L, et al. Nanoparticles modified by encapsulation of ligands with a long alkyl chain to affect multispecific and multimodal imaging. *J Nucl Med*. 2012;53(9): 1462–1470.
22. Madru R, Kjellman P, Olsson F, et al. 99mTc-labeled superparamagnetic iron oxide nanoparticles for multimodality SPECT/ MRI of sentinel lymph nodes. *J Nucl Med*. 2012;53(3):459–463.
23. Yang X, Hong H, Grailer JJ, et al. cRGD-functionalized, DOX-conjugated, and (6)(4)Cu-labeled superparamagnetic iron oxide nanoparticles for targeted anticancer drug delivery and PET/MR imaging. *Biomaterials*. 2011;32(17):4151–4160.
24. Schwochau K. Technetium radiopharmaceuticals—fundamentals, synthesis, structure, and development. *Angew Chem Int Ed Engl*. 1994;33(22):2258–2267.
25. Matsunaga K, Hara K, Imamura T, Fujioka T, Takata J, Karube Y. Technetium labeling of dextran incorporating cysteamine as a ligand. *Nucl Med Biol*. 2005;32(3):279–285.
26. Jung CW, Jacobs P. Physical and chemical properties of superparamagnetic iron oxide Mr contrast agents—ferumoxides, ferumoxtran, ferumoxsil. *Magn Reson Imaging*. 1995;13(5):661–674.
27. Guo Y, Zhang Y, Jin N, et al. Electroporation-mediated transcatheter arterial chemoembolization in the rabbit VX2 liver tumor model. *Invest Radiol*. 2012;47(2):116–120.
28. Kim YI, Chung JW, Park JH, Han JK, Hong JW, Chung H. Intraarterial gene delivery in rabbit hepatic tumors: transfection with nonviral vector by using iodized oil emulsion. *Radiology*. 2006;240(3):771–777.
29. Kim KW, Lee JM, Kim JH, et al. CT color mapping of the arterial enhancement fraction of VX2 carcinoma implanted in rabbit liver: comparison with perfusion CT. *AJR Am J Roentgenol*. 2011;196(1):102–108.
30. Jeong JM, Hong MK, Kim YJ, et al. Development of Tc-99m-neomannosyl human serum albumin (Tc-99m-MSA) as a novel receptor binding agent for sentinel lymph node imaging. *Nucl Med Commun*. 2004;25(12):1211–1217.
31. Chang IS, Lee MW, Kim YI, et al. Comparison between transauricular and transfemoral arterial access for hepatic artery angiography in a rabbit model. *J Vasc Interv Radiol*. 2011;22(8): 1181–1187.
32. Lee IJ, Kim YI, Kim KW, et al. Radiofrequency ablation combined with transcatheter arterial embolisation in rabbit liver: investigation of the ablation zone according to the time interval between the two therapies. *Br J Radiol*. 2012;85(1019): e987–e994.
33. Xing Y, Zhao JH, Conti PS, Chen K. Radiolabeled nanoparticles for multimodality tumor imaging. *Theranostics*. 2014;4(3): 290–306.
34. Miyayama S, Matsui O, Yamashiro M, et al. Ultraselective transcatheter arterial chemoembolization with a 2-f tip microcatheter for small hepatocellular carcinomas: relationship between local tumor recurrence and visualization of the portal vein with iodized oil. *J Vasc Interv Radiol*. 2007;18(3):365–376.
35. Di Martino M, Marin D, Guerrisi A, et al. Intraindividual comparison of gadoxetate disodium-enhanced MR imaging and 64-section multidetector CT in the Detection of hepatocellular carcinoma in patients with cirrhosis. *Radiology*. 2010; 256(3):806–816.
36. De Santis M, Alborino S, Tartoni PL, Torricelli P, Casolo A, Romagnoli R. Effects of lipiodol retention on MRI signal intensity from hepatocellular carcinoma and surrounding liver treated by chemoembolization. *Eur Radiol*. 1997;7(1):10–16.